Journal of Molecular Structure 1247 (2022) 131420

Contents lists available at ScienceDirect

Journal of Molecular Structure

journal homepage: www.elsevier.com/locate/molstr

Docking of disordered independent molecules of novel crystal structure of (N-(4-methoxyphenyl)-2-(3-methyl-2-oxo-3,4-dihydroquinoxalin-1(2H)-yl)acetamide as anti-COVID-19 and anti-Alzheimer's disease. Crystal structure, HSA/DFT/XRD

Mohcine Missioui[a], Musa A. Said[b], Güneş Demirtaş[c], Joel T. Mague[d], Youssef Ramli[a,*]

[a] Laboratory of Medicinal Chemistry, Drug Sciences Research Center, Faculty of Medicine and Pharmacy, Mohammed V University in Rabat, Morocco
[b] Chemistry Department, College of Science, Taibah University, PO Box 30002, Al-Madinah Al Munawarah Code 1417, Saudi Arabia
[c] Ondokuz Mayıs University, Faculty of Arts and Sciences, Department of Physics, Samsun 55139, Turkey
[d] Department of Chemistry, Tulane University, New Orleans, LA 70118, USA

ARTICLE INFO

Article history:
Received 18 May 2021
Revised 20 August 2021
Accepted 31 August 2021
Available online 3 September 2021

Keywords:
Quinoxaline
Crystal structure
Gap energy
DFT
Hirshfeld surface analysis (HSA)
In silico molecular docking
COVID- 19
Alzheimer's disease

ABSTRACT

New quinoxaline derivative, N-(4-methyl-2-nitrophenyl)-2-(3-methyl-2-oxoquinoxalin-1(2H)-yl)acetamide (NMPOQA= disordered molecules NMPOQAa(50.3% and NMPOQAb(49.7%)) has been synthesized and characterized by ESI-MS, IR, ^{1}H &^{13}C NMR. The geometric parameters of NMPOQA compound which crystallographic structure has been defined by X-ray diffraction have been calculated by Density Functional Theory (DFT), B3LYP, 6-311++G(d,p) basis set. The correlation between experimental and theoretical structure was checked by superimposing the experimental and theoretical structure. Frontier Molecular Orbitals (FMO's) have been created and the gap energy between High Occupied Molecular Orbital (HOMO) and Low Unoccupied Molecular Orbital (LUMO) has been calculated. Additionally, Molecular Electrostatic Potential (MEP) and Hirshfeld studies have been conducted to analyze intermolecular interactions. Interesting molecular docking of NMPOQA and Remdesivir drug with 6M03 was conducted using the same parameters for a fair comparison. A low binding affinity of the NMPOQA (−6.9 kcal/mol) compared to the Remdesivir drug, (−7.1 kcal/mol) and other good reasons make NMPOQA a good candidate against COVID-19. A similar study was calculated with 1EVE producing evidences that suggest NMPOQA may serve as a potential drug for developing Alzheimer's disease (AD) treatment

1. Introduction

The Coronavirus Disease 2019 (COVID-19) pandemic, Severe Acute Respiratory Syndrome coronavirus 2 (SARS-CoV-2) infection that causes the current global health crisis, is a worldwide concern affecting all countries. As of 17 May 2021, there have been 163.218.483 confirmed cases of this disease, including 3.384.668 deaths in 216 countries, reported to the World Health Organization (WHO). With the prevalence of Covid-19, the risks of neurological disease need to be carefully evaluated for neurologists and a study reported that affected patients may be at high risk of developing Alzheimer's disease (AD) after overcoming the SARS-CoV-2 infection [1]. Researchers reported SARS-CoV-2 can disrupt angiotensin-converting enzyme type 2 (ACE2) signaling pathway cause neurodegeneration of dopaminergic neurons or impairment in cholinergic pathways, and may involve in the progression of AD [2]. Several reports suggested a beneficial effect of traditional medicine (TM)/herbal medicines (HMs), in COVID-19 [3–6]. Similarly, proposed agents to treat COVID-19 include direct antivirals [7], hydroxychloroquine [8], baricitinib [9], glucocorticoids [10] and anakinra [11,12] Currently, several molecules are being tested for their efficacy on COVID-19 disease, some of which have reached clinical trials, while others are still in preclinical phase [13–17]. While the use of corticoids and other immunomodulators has been controversial [18–22]. In this case, the U.S. Food and Drug Administration (FDA) approved only remdesivir for the treatment of COVID-19 [23]. So far, there is no permanent remedy for AD, there are only well-stated hypotheses and concepts about the cause and drug targets of AD. The chemistry of quinoxaline has attracted the attention of researchers due to its diversity in different applications, from a wide spectrum of biological proprieties to materials science [24–26]. Hence, quinoxaline as a wonder nucleus in the fused systems of nitrogen-containing heterocycles always shows

* Corresponding author.
E-mail address: y.ramli@um5s.net.ma (Y. Ramli).

https://doi.org/10.1016/j.molstruc.2021.131420
0022-2860/

a variety of activities in the medical field [27–32], especially antivirals [33,34]. Multi-targeted drugs can be looked forward to for dealing with symptoms of the disease. b-Site amyloid precursor protein cleaving enzyme 1 (BACE1) has been the primary therapeutic target for AD therapies, against Ab accumulation. However, all the potential drugs developed have not been successful beyond phase II/III trials [35]. The SARS-CoV-2 main protease plays an important role in viral replication. In fact, it is a key target for COVID-19 drug discovery. Other important roles in understanding the molecular mechanism in drug discovery are the binding affinity and structure of protein–drug complexes. Since COVID-19 is not a rare disease, the development of other more scalable treatments is still of great importance. Notably, a new candidate to inhibit binding between the COVID-19 main protease and the angiotensin converting enzyme-2, on the cell surface. The purpose of the current work is to synthesize a new quinoxaline-*N*-arylacetamide hybrid system and screen, *in silico*, the interaction between the main protease active site with this novel quioxaline derivative NMPOQA. Also, *in silico* anti-dementia, related to Alzheimer's disease, activity prediction was examined, so, in continuation of our recent work focused on the synthesis and biological evaluation of novel heterocyclic compounds [36–41], herein, our results are presented.

2. Experimental section

2.1. Synthesis

From Sigma-Aldrich we purchased the chemicals and solvents for the synthesis of the main compounds. The reaction advancement was supervised via thin-layer chromatography. The melting point was obtained on a Büchi Melting Point SMP-20 apparatus and is uncorrected. The ^{1}H NMR and ^{13}C NMR spectra were recorded on a Bruker Avance 300 NMR Spectrometer in DMSO-d6. The chemical shifts δ are reported in parts per million (ppm); the IR spectrum was obtained using the Bruker-VERTEX 70 device and the associated software OPUS, in ATR (attenuated total reflectance) mode. Mass spectra were recorded on an API 3200 LC/MS/MS mass spectrometer using electrospray ionization (ESI) in positive polarity.

2.1.1. 3-Methyl-1H-quinoxalin-2-one (MQO)

Following a procedure similar to that of Hinsberg [42], we have successfully synthesized 3-methyl-1*H*-quinoxalin-2-one, by condensation of *O*-phenylenediamine (10 mmol) with ethyl pyruvate (15 mmol) in HCl aqueous solution for 30 minutes at room temperature (Scheme 1).

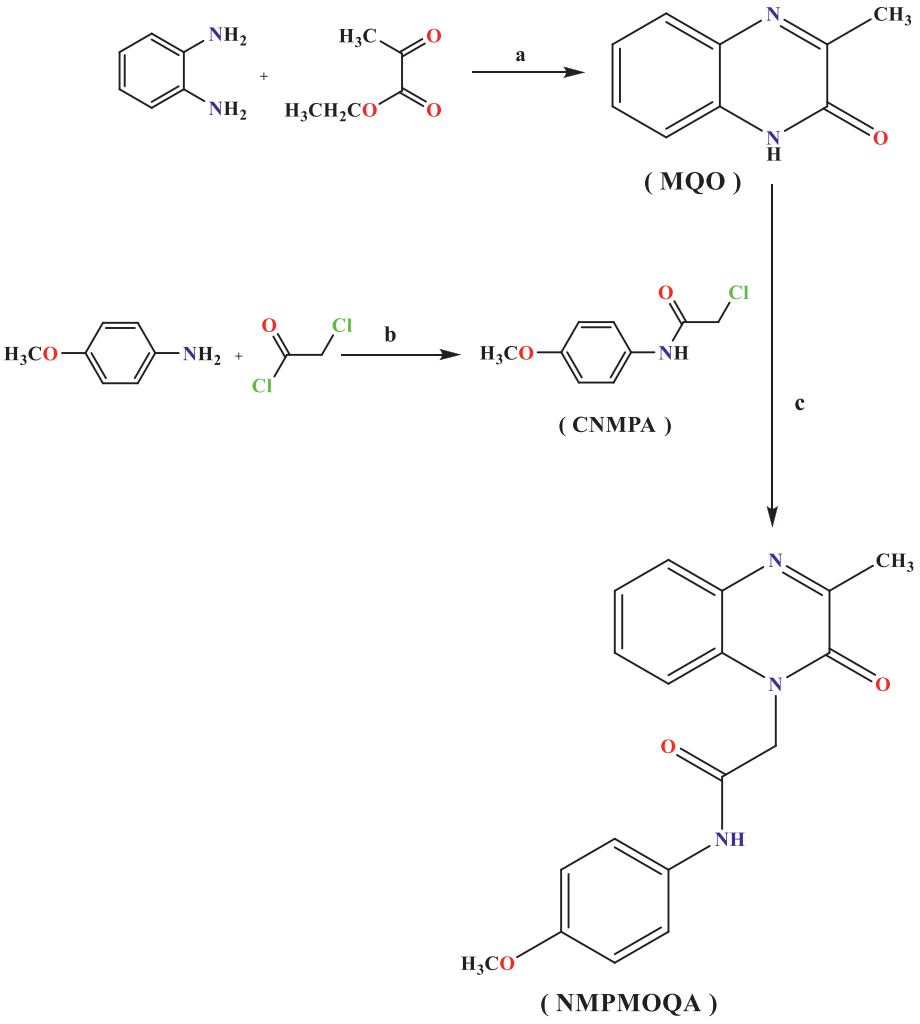

Scheme 1. Synthesis procedure for preparation of (NMPOQA);Reagents : (a) HCl 4N; (b) Acetic acid glacial; (c) K_2CO_3, BTBA, DMF.

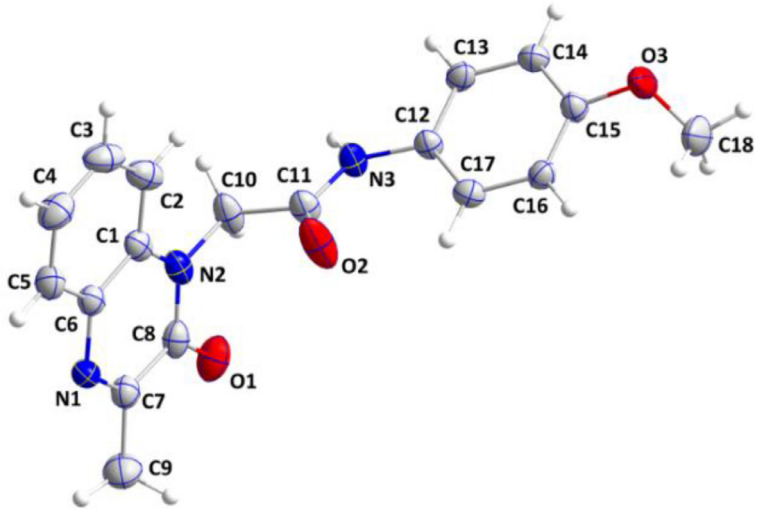

Fig. 1. ORTEP view of the molecular structure of NMPOQA with labeling scheme and 50% probability ellipsoids.

2.1.2. 2-Chloro-N-(4-methoxyphenyl)acetamide (CNMPA)

A (0.047 moles) of P-Toluidine was dissolved in 40 mL of pure acetic acid and put in an ice bath. Then, chloroacetyl chloride (0.047 moles) was added portion-wise with stirring, in the end of the reaction a solution of sodium acetate (35 mL) was added, a solid precipitation will appear after 30 min of stirring at room temperature, the resulting solid was filtered and washed with cold water, dried and recrystallized from ethanol to give compound CNMPA. (Scheme 1)

2.1.3. N-(4-methoxyphenyl)-2-(3-methyl-2-oxoquinoxalin-1(2H)-yl)acetamide (NMPOQA)

we dissolved (3g, 18,5 mmol) of 3-methylquinoxalin-2(1H)-one in dimethylformamide, then we added (5,5 g, 27,7 mmol) of 2-chloro-N-(4-methyl-2-nitrophenyl)acetamide previously prepared, for the proton removal we use as a base a (2,5 g, 18,6 mmol) of potassium bicarbonate, and a tip of spatula of BTBA was used for the phase transfer catalysis, then, under reflux, the reaction was stirred for 2 hours at 80°C. When the starting reagents have completely reacted, 500 ml of distilled water was added, few minutes later the product precipitated in a solid form then filtered dried and recrystallized from hot ethanol. (Scheme 1)

2.2. Single crystal X-ray structure determination

A colorless plate-like specimen of $C_{18}H_{17}N_3O_3$, approximate dimensions 0.030 mm x 0.173 mm x 0.204 mm, was used for the X-ray crystallographic analysis. The X-ray intensity data were measured at 150 K on a Bruker D8 VENTURE PHOTON 100 CMOS system equipped with a INCOATEC IμS micro-focus source (Cu-Kα, λ = 1.54178 Å) and a mirror monochromator. The complete sphere of data was processed using SAINT [43]. The structure (Fig. 1) was solved by direct methods and refined by the full-matrix least-squares method on F2 using SHELXT and SHELXL programs [44,45]. The molecular and packing diagrams were generated using DIAMOND [46]. Crystal and refinement details are presented in Table 1.

CCDC 2061622 contains the supplementary crystallographic data for this paper. These data can be obtained free of charge via http://www.ccdc.cam.ac.uk/conts/retrieving.html (or from the Cambridge Crystallographic Data Centre, 12, Union Road, Cambridge CB2 1EZ, UK; fax: +44 1223 336033).

Table 1
Crystal data and structure refinement details.

Value	Parameter
Chemical formula	$C_{18}H_{17}N_3O_3$
M_r	323.34
Crystal system, space group	Triclinic, *P-1*
Temperature (K)	150
a, *b*, *c* (Å)	4.6859 (2), 9.4248 (5), 18.5551 (9)
α, β, γ (°)	78.670 (3), 84.647 (3), 76.694 (3)
V (Å^3)	780.93 (7)
Z	2
Radiation type	Cu *K*α
μ (mm^{-1})	0.78
Crystal size (mm)	0.20 × 0.17 × 0.03
Diffractometer	Bruker D8 VENTURE PHOTON 100 CMOS
Absorption correction	Multi-scan *TWINABS* (Sheldrick, 2009) [47]
T_{min}, T_{max}	0.86, 0.98
No. of measured, independent and observed [$I > 2\sigma(I)$] reflections	7159, 7159, 5450
R_{int}	0.038
(sin $\theta/\lambda)_{max}$ (Å^{-1})	0.610
$R[F^2 > 2\sigma(F^2)]$, $wR(F^2)$, S	0.057, 0.147, 1.01
No. of reflections	7159
No. of parameters	216
No. of restraints	2
H-atom treatment	H-atom parameters constrained
$\Delta\rho_{max}$, $\Delta\rho_{min}$ (e Å^{-3})	0.32, −0.21

2.3. Computational procedure

Theoretical results about the molecule were carried out using Gaussian 03 package program [48]. For this operation, Density Functional Theory (DFT) by B3LYP with 6-311++G(d,p) basis set was used. The data obtained X-ray diffraction was used as initial values for the calculation. Molecular orbitals and molecular electrostatic potential map were created with Gauss-View molecular visualization program [49].

Hirshfeld surfaces analysis (HAS) and the related 2D-fingerprint plots were calculated for (NMPOQA), using Crystal Explorer, Version 17 which reads a crystal structure input file as CIF format [50]. The cut-off for the non-bonded interactions, without the hydrogen atoms, between the amino acid residues and the ligand, for the LIGPLOTs that appeared in this paper, is 3.9 Å [51].

2.4. *Docking* in silico *studies*

Docking calculations of the NMPOQA and drugs were accomplished using the Autodock Vina wizard in PyRx 0.8 [52] (available freely from https://sourceforge.net/projects/pyrx/). It is a powerful visualization engine and valuable software for molecular docking [53]. Both the occupancies of the disordered title ligand crystal 0.503(2) NMPOQAa /0.497(2) NMPOQAb binding modes of the NMPOQA (a and b) under the same conditions have been explored for comparison. Settings in the program include: Grid box center_x = 12.117, center_y = -11.3843, center_z = 4.6603, size_x = 25, size_y = 25 and size_z = 25 for the NMPOQA against Remdesivir drug. Whereas the grid box for the NMPOQA against the Donepizl drug is: center_x = 5.0229, center_y = 65.044, center_z = 55.8104, size_x = 25, size_y = 25 andsize_z = 25. The exhaustiveness for all is 8. The energy minimization of the ligand and protein was performed using the default settings in the Autodock Vina-PyRx. The CIF files of the NMPOQA (CCDC= 2061622), Donepizl (CCDC= 1525480) and Remdesivir (CCDC= 1438375) were converted to PDB file type using Biovia Discovery Studio 4.5 [54] and were introduced as input to Autodock vina in PyRx. The proteases (PDB code 1EVE and 6M03) were saved in PDB format after deletion of the water molecules and ligands. Schematic diagrams of protein-ligand interactions were generated using the LIGPLOT program [55].The PyMOL molecular viewer was used to present the output [56].

3. Results and discussion

3.1. Synthesis

The synthesis of the compound (NMPOQA) is depicted in Scheme 1. The starting material, 3-methylquinoxalin-2(1*H*)- one was prepared through treatment of *o*-phenylenediamine with ethyl pyruvate in acetic acid [42]. This compound was proven to be a good synthon for different highly biologically active compounds. The lactam function of quinoxalinone is very reactive and so it is condensed with 2-chloro-*N*-(4-methoxyphenyl)acetamide (CNMPA). The structure of NMPOQA was elucidated the based on spectral data.

3.1.1. 3-Methyl-1H-quinoxalin-2-one (MQO)

Yield 91%, mp=219.3-220.5°C, FT-IR (ATR, υ, cm-1) 1568 υ (C=N), 1663 υ (C=O), 2710, 2843, 2898, 2963, 3007 υ(C-H, aromatic), 3430 υ (N-H). ^{1}H NMR (DMSO-d_6) δ ppm: 2.40 (3H, s, CH_3), 7.27 (2H, m, H_{arom}), 7.28 (1H, d, J = 8.86 Hz, H $_{arom}$), 12.29 (1H, s, N-H). ^{13}C NMR (DMSO-d_6) δppm: 20.51 (CH_3), 115.22, 123.04, 127.86, 129.31 (C-H_{Arom}), 131.65 (C_{arom}-N), 131.91 (C_{arom}-N), 159.22 (C=O); HRMS (ESI-MS) (m/z) calculated for $C_9H_8N_2O$ 160.06, found 160.17

3.1.2. 2-Chloro-N-(4-methoxyphenyl)acetamide (CNMPA)

Yield 80%, color: beige, mp=125.6-127.3°C, R_f, FT-IR (ATR, v, cm-1) 3292 v (N-H amide), 1029 v (N-C amide), 1660 v (C=O amide), 3073 v(C-H_{arom}), 827 v(C-Cl), 2959 v(C-H,CH_2), ^{1}H NMR (DMSO-d_6) ppm: 3.74 (3H, s, CH_3); 4.24 (2H, s, CH_2), 6.93-7.5 (4H, m, *J* =1.3Hz, H_{arom}), 10.23 (1H, s, NH), ^{13}C NMR (DMSO-d_6) δ ppm: 43.48 (CH_2), 55.23 (CH_3), 131.53 (C_{arom}-N), 155.51 (C_{arom} -O), 113.92–120.92 (C_{Arom}); 164.13 (C=O); HRMS (ESI-MS) (m/z) calculated for $C_9H_{10}ClNO$ 183,64, found 184.0105

3.1.3. N-(4-methoxyphenyl)-2-(3-methyl-2-oxoquinoxalin-1 (2H)-yl)acetamide (NMPOQA)

Yield 85%, color : beige, mp= 166.5–168.3°C, FT-IR (ATR, υ, cm^{-1}): 3251 υ(N-H_{amide}); 1651 υ(C=O_{amide}); 752 υ(C-H_{arom}); 1539 υ(C=C_{arom}); 1470 υ(C-H $_{CH3}$);); 1215 υ(C-$O_{methoxy}$); ^{1}H NMR (DMSO-d_6) δ ppm: 2.49 (3H, s, $CH_{3,quin}$); 3.73 (3H, s, CH_3 $_{methoxy}$); 5.11 (2H, s, CH_2); 10.32 (1H, s, NH); 6.75–7.82 (m, *J*=7.3 Hz, 8H_{Ar}); ^{13}C NMR (DMSO-d_6) δppm: 55.14 (CH_2); 45.30 (CH_3 $_{methoxy}$); 21.09 (CH_3 $_{quin}$); 164.26 (C-O); 165.53 (C=$O_{acetamid}$); HRMS (ESI-MS) (m/z) calculated for $C_{18}H_{17}N_3O_3$ 323,13 found 324.12936

Based on of ^{1}H NMR spectrum of NMPOQA which exhibited four signals at δ 2.49, 3.73, 5.11 and 10.64 ppm referring to a methyl group, CH_3 of the methoxy group, CH_2 bound to the quinoxaline nitrogen and NH of acetamide group respectively. Besides, we revealed the absence of a signal at δ 12.29 ppm corresponding hydrogen of the lactam which confirms the reaction between 3-methylquinoxalin-2(1H)-one and 2-chloro-N-(4-methoxyphenyl)acetamide. Regarding the ^{13}C NMR spectrum, there are signals at 21.09 ppm, 45.30 ppm, 55.14 ppm, 164.26 ppm and 165.63 ppm referring to the carbon of, the CH_3 group linked to the quinoxaline entity, the CH_3 of the methoxy group, the CH_2 entity, the carbon linked to the oxygen of methoxy group and finally the carbon of acetamide group respectively. The presence of the characteristic signals of the precursors simultaneously confirms the structure of our compound. Concerning the FT-IR spectrum, it shows mainly characteristic peaks at 3251 υ, 1651 υ and 1215 υ referring respectively to the C=O bond of the amide entity, the NH bond of acetamide group, and finely the C-O bond of methoxy entity. Its mass spectrum showed a molecular ion peak (MH^+, m/z = 324,129) which conforms to its molecular formula $C_{18}H_{17}N_3O_3$. SM (ESI+), IR and NMR spectra are given in the Supplementary Material Tables S1–S3.

Table 2
Hydrogen-bond geometry (Å, °).

Cg2 is the centroid of the C1··· C6 benzene ring.

D—H···A	D—H	H···A	D···A	D—H···A
N3—H3A···O2^i	0.91	1.90	2.801 (3)	170
C10—H10A··· Cg2^i	0.99	2.78	3.571 (4)	137

Symmetry code: (i) x+1, y, z.

3.2. Single crystal X-ray structure determination

The conformation of the molecule can be described as a "spatula" with the dihydroquinoxaline unit as the blade and the long side chain as the handle (Fig. 1). The dihydroquinoxaline portion is not quite planar as indicated by the 2.58(17)° dihedral angle between its constituent planes. The C10/C11/O2/N3 unit of the side chain is nearly perpendicular to the mean plane of the dihydroquinoxaline moiety as indicated by the C8—N2—C10—C11 torsion angle of -96.95 (30)°. In the side chain, the C12···C17 benzene ring is rotationally disordered over two sites 52.3 (2)° apart in a 0.503 (2)/0.497(2) ratio with the slightly larger component making an 86.0 (1)° dihedral angle with the mean plane of the C1/C6/N1/C7/C8/N2 ring. In the crystal, N3—H3A···O1 hydrogen bonds abetted by C10—H10A···Cg2 interactions (Table 2) form chains of molecules extending along the a-axis direction (Fig. S4, Supplementary Materials). The chains pack across inversion centers with normal van der Waals contacts (are also shown in Supplementary Materials Figs. S5 and S6).

3.3. Computational study

3.3.1. Geometric optimization of the compound

In this study, the theoretical structure of the compound NMPOQA was calculated using DFT/B3LYP, 6-311++G(d,p) method. Because of having a disorder, calculations were only figured out for the situation that the benzene group is almost perpendicular to 3-methylquinoxalin-2(1*H*)-one group. For initial values, this

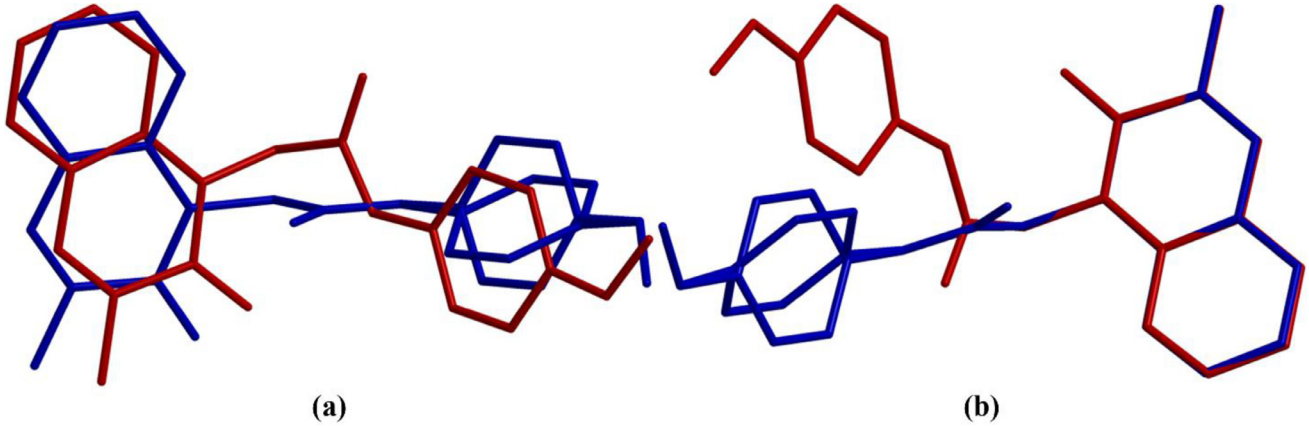

Fig. 2. Superposition of experimental structure (blue) and theoretical structure (red). (a) Superposition for all atoms (RMS=1.292 Å), (b) superposition for C1-C11, N1, N2 atoms (RMS=0.108 Å).

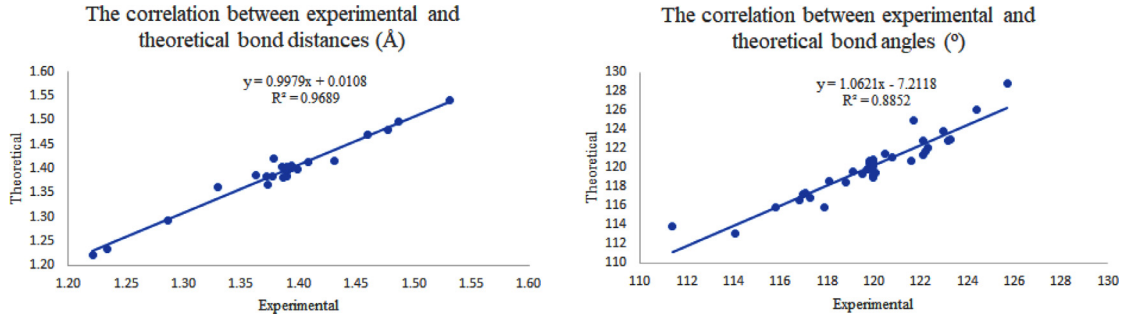

Fig. 3. The correlation values between experimental and theoretical geometrical parameters.

angle between benzene (C12, C13, C14, C15, C16, C17) and 3-methylquinoxalin-2(1*H*)-one group is 86.59°. In the molecule, the angle between the benzene group created by disordered atoms (C12A, C13A, C14A, C15A, C16A, C17A) and 3-methylquinoxalin-2(1*H*)-one group is 60.76°.

After calculation, the angle between the plane created by the benzene ring and the plane created by 3-methylquinoxalin-2(1*H*)-one group was calculated as 62.13°. Total energy for this orientation of molecule was obtained as -1086.4074 a.u. The molecule adopts the orientation created by disordered atoms, since the molecule was calculated in gas phase. In Fig. 2, theoretical and experimental geometries were superimposed on each other. As can be seen in Fig. 2, the theoretical structure doesn't completely overlap with the experimental structure.

If the bond distances and bond angles are considered, both theoretical bond distances and bond angles close to experimental values. For bond distances, while the least difference was found for O1-C8 with 0.0001 Å error, the biggest difference was found for O3-C18 with -0.0425 Å error value. RMSE and R^2 results are 0.0142 Å and 0.9689, respectively (Table 3) . While the calculated geometric parameters with experimental parameters are given in Table 4 and Table 5, the linear correlations between these results are given graphically in Fig. 3.

For bond angles, while the biggest difference was found for O3-C15-C16 bond angle with -3.2005°, the least difference was found for N2-C8-C7 bond angle with -0.0170° error value.

The N2—C10—C11—O2 and C12—N3—C11—O2 torsion angles obtained X-ray diffraction are -1.1(5)° and 1.8(5)°, respectively. These torsion angles calculated by DFT are -109.0708° for N2—C10—C11—O2 and 2.0951° for C12—N3—C11—O2. Although the theoretical results close to the experimental results, the theoretical and the experimental structure do not completely overlap.

3.3.2. Molecular electrostatic map

DFT/B3LYP/6-311++G (d,p) basis set was used to generate Molecular Electrostatic Potential (MEP) of the molecule. MEP which gives information about intermolecular interactions of molecules contains blue and red areas which show nucleophilic and electrophilic attack centers, respectively. As can be seen in Fig. 4, electrophilic attack centers concentrate on the environment of oxygen atoms. Electrostatic charge values for these regions are approximately -0.0368 a.u. for O1 atom, -0.0454 a.u. for O2 atom and -0.0309 a.u. for O3 atom. In addition to oxygen atoms, the value for the environment of N1 atom is -0.0300 a.u. These values point out intermolecular interactions at the environment of oxygen atoms. X-ray data confirms MEP that the crystal structure has an intermolecular N3—H3A···O2 hydrogen bond. However, the molecule has minimum energy where an intramolecular hydrogen bond is created between N3 and O1 atoms, due to the conformation of the molecule.

3.3.3. Hirshfeld surface analysis

HSA plays a key role in showing the inter-and intra-molecular interactions in the crystal structure. The mesh drawing and short interaction were studied by Hirshfeld surface generated using Crystal Explorer [52]. The red circle on d_{norm} Hirshfeld surface indicates the presence of π-π stacking, which corresponds to the ph-ph and quinoxalin- quinoxalin interaction shown in Fig. 5(b). N3—H3—O2 and C14—H14—H18 hydrogen bonds as shown in Fig. 5(a). The Hirshfeld surface analysis of the NMPOQAa shows H—H interaction contributes 43.30% which plays an important role in stabilizing the crystal structure, whereas the C—H interaction contributes 25.3%. The O—H interaction contributes 20. 50%. All 2D-finger plots and the percentage contributions of various interactions are shown in Fig. 5(a).

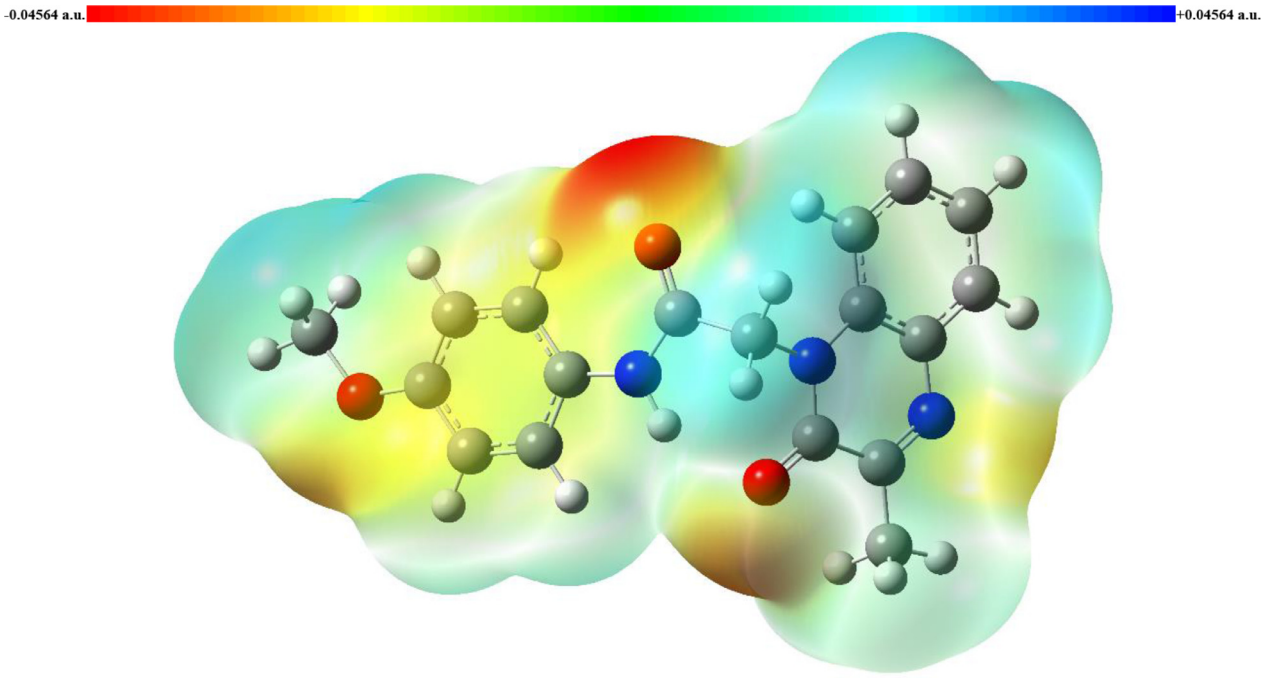

Fig. 4. The molecular electrostatic potential (MEP) map of the molecule.

Table 3
Experimental and theoretical bond distances of the title compound (Å).

Bond Distances							
Atoms	X-ray	DFT	Error	Atoms	X-ray	DFT	Error
O1-C8	1.234(3)	1.2339	0.0001	C4-C5	1.377(4)	1.3826	-0.0056
O2-C11	1.221(3)	1.2222	-0.0012	C5-C6	1.394(4)	1.4051	-0.0111
O3-C15A	1.369((3)	-	-	C7-C8	1.478(4)	1.4810	-0.0030
O3-C15	1.373(3)	1.3667	0.0063	C7-C9	1.487(4)	1.4977	-0.0107
O3-C18	1.378(4)	1.4205	-0.0425	C10-C11	1.531(4)	1.5405	-0.0095
N1-C7	1.287(4)	1.2926	-0.0056	C12-C13	1.39	1.4042	-0.0142
N1-C6	1.387(4)	1.3818	0.0052	C12-C17	1.39	1.3955	-0.0055
N2-C8	1.372(4)	1.3842	-0.0122	C13-C14	1.39	1.3836	0.0064
N2-C1	1.399(4)	1.3975	0.0015	C14-C15	1.39	1.4003	-0.0103
N2-C10	1.460(4)	1.4710	-0.0110	C15-C16	1.39	1.3947	-0.0047
N3-C11	1.330(3)	1.3612	-0.0312	C16-C17	1.39	1.3973	-0.0073
N3-C12A	1.429(3)	-	-	C12A-C13A	1.39	-	-
N3-C12	1.431(3)	1.4150	0.0160	C12A-C17A	1.39	-	-
C1-C2	1.386(4)	1.4036	-0.0176	C13A-C14A	1.39	-	-
C1-C6	1.408(4)	1.4145	-0.0065	C14A-C15A	1.39	-	-
C2-C3	1.363(5)	1.3870	-0.0240	C15A-C16A	1.39	-	-
C3-C4	1.394(5)	1.4013	-0.0073	C16A-C17A	1.39	-	-

3.3.4. Frontier molecular orbitals

Frontier Molecular Orbitals (FMO's) were created using the same level theory. High Occupied Molecular Orbital (HOMO) and Low Unoccupied Molecular Orbital (LUMO) with the gap energy belong to the compound are given in Fig. 6. Molecular orbitals which are occupied by electrons define chemical activity of molecules and Frontier Molecular Orbitals are very important in terms of chemical, electrical and optical properties of compounds [57]. HOMO and LUMO from these orbitals identify ionization energy and electron affinity, respectively [58]. Gap energy between HOMO and LUMO is related to electron conductivity, molecular transport properties, biological activity and chemical stability, photo stability and [59,60]. While HOMO orbital distributes on N-(4-methoxyphenyl)formamide group of the molecule, LUMO distributes mainly on 3-methylquinoxalin-2(1H)-one group. The gap energy between these orbitals is calculated as 3.4841 eV. This value shows that the molecule has high chemical stability.

3.4. Docking analysis

3.4.1. Docking against 1EVE

This docking study aims to examine how the (N-(4-methoxyphenyl)-2-(3-methyl-2-oxo-3,4-dihydroquinoxalin-1(2H)-yl)acetamide) NMPOQAa, in its different components; might bind with the TcAChE enzyme (PDB, 1EVE) as a likely drug for Alzheimer's disease. The docked NMPOQAa has interacted with the active site of 1EVE as shown in Fig. 7. Superimposition of NMPOQA and donepezil are shown in Fig. 7(a) representing the structure of the protein–drug complex framework within the active site of 1EVE protease. The interactions of the donepezil and NMPOQA against the AChE (1EVE) are formed through hydrophobic interactions between the ligand and the active amino acid residues of the receptor, mainly via the $\pi\cdots\pi$ stacking and the lone pair of electrons on the O and N atoms. The display of the docking result shows an overlapping of NPOQAa and NPOQAb with a small

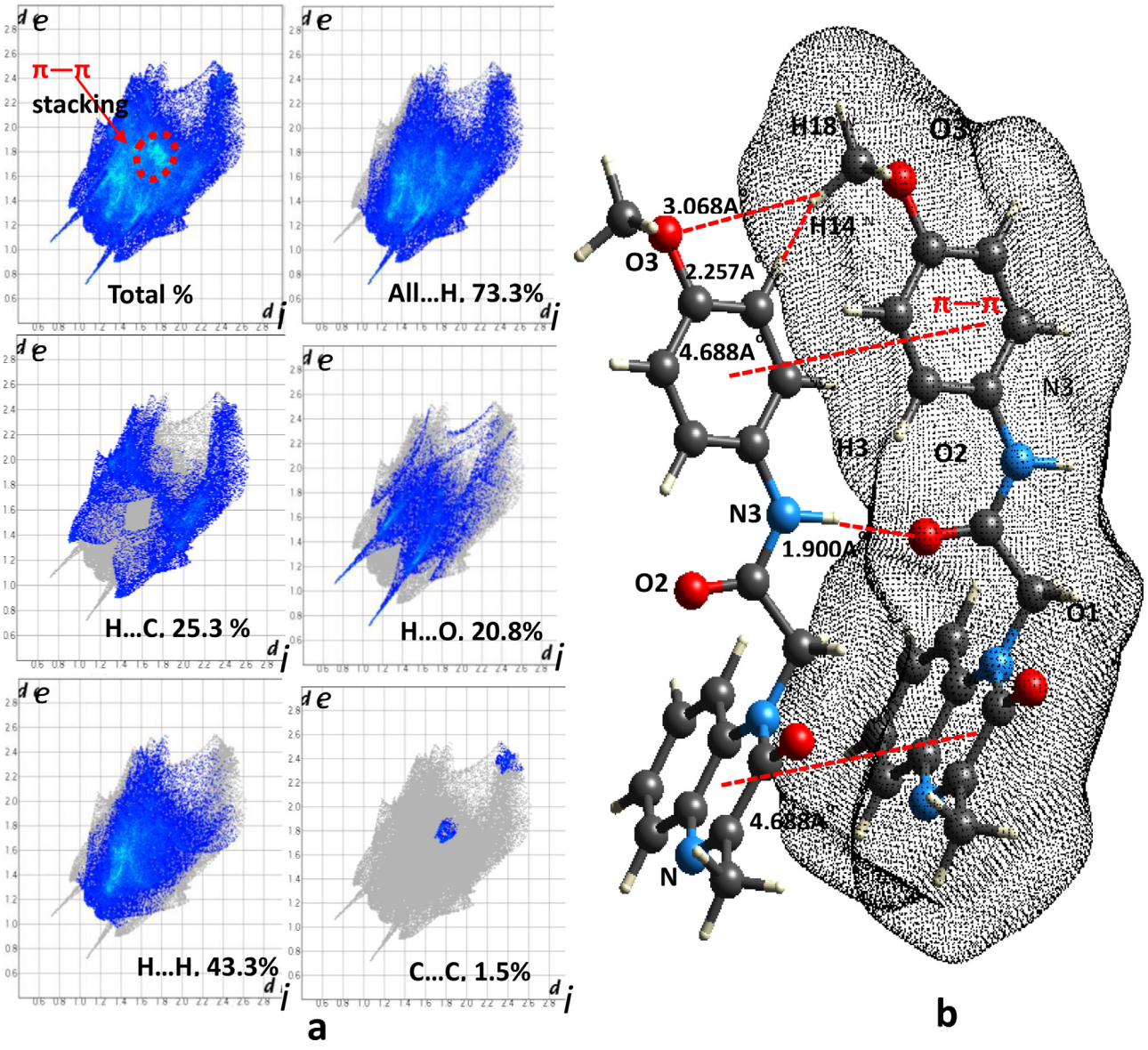

Fig. 5. Hirshfeld surface fingerprint (2D) plots of the closest internal distance (d_i) versus the closest external distance analysis (d_e) for NMPOQAa, major component, d_i and d_e refer to intra- and intermolecular contacts, respectively; (b)A mesh presentation of the NMPOQAa showing the electron density around all the atoms of the molecule using the CrystalExplorer program with CIF data. Short contacts are presented by red dashes (H-bonds and $\pi-\pi$ stacking).

noticeable difference, Fig. 7(c). The difference is much manifested in the binding affinities represented in Fig. 8 for all possible conformations of the NMPOQA. Only the first pose for both the independent molecules shows equal binding energy (-8.1 kcal/mol, NMPOQA +1EVE and -6.9 kcal/mol, NMPOQA +6M03), whereas the remaining 8 poses are different for both, Fig. 8. This indicates that both the molecules NMPOQA ((a) and (b)) do not behave fully the same in docking against 1EVE and 6M03 proteases, Fig. 8. Interestingly, the NPOQA appeared to occupy the same space as the Donepezil drug Fig. 7(b). The binding affinity for our ligand in this study against the Torpedo California acetylcholinesterase (TcAChE), (PDB, 1EVE) is related to the number of hydrogen bonding and hydrophobic interactions, that is comparable to the Donepezil drug (-11.1 kcal/mol, obtained under similar conditions as for NMPOQA in this study) creating hope to be a possible selective acetylcholinesterase inhibitor. Furthermore, Donepezil drug and NMPOQAa have many common interactions in common, Fig. 9(a): (Glu69, Tyr70, Trp84, Gly118, Tyr121, Ser122, Glu199, Ser200, Phe330, Phe331 and his440). The interaction of donepezil drug and NMPOQAa against AChE (1EVE) demonstrations H-bonds; Asp72 (3.34 Aº) for NMPOQAa and Gly118 (2.77 Aº) and Trp (3.14 Aº) for donepezil drug Fig. 9(a). It is documented that, Trp84, an active amino acid residue of the receptor was recognized as the main component of the anionic site [61] which is present in both the cases in this study. The bottom of the gorge, $\pi-\pi$ hydrophobic interaction was also observed between one ring of donepezil and NMPOQA with the phenyl of His440(A) in the active amino acid residues of AChE [62]. Hence, in summary, two strong reasons might propose that our ligand may serve as a potential drug for treating AD; (i) The low docking score of the NMPOQA (-8.1 kcal/mol) and (ii) The many common interaction residues found between the NMPOQA against AChE (1EVE), from one side, and the standard donepezil drug against AChE (1EVE).

3.4.2. Docking against 6M03

In this part of the docking study, at this very critical time, it is interesting to examine how an acetamide -based ligand might approach the active site of the main protease for Covid-

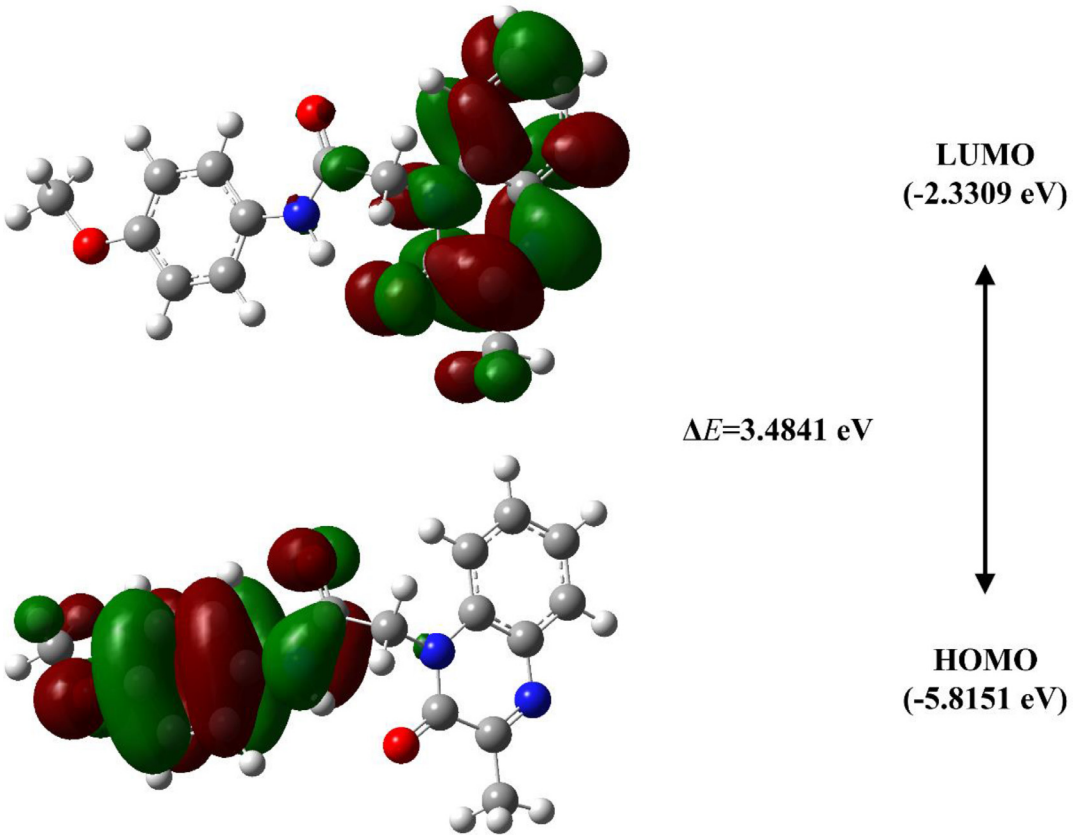

Fig. 6. Frontier molecular orbitals of the compound NMPOQA.

Table 4
The experimental and theoretical bond angles of the title compound (°).

Bond Angles					
Atoms	X-ray	DFT	Atoms	X-ray	DFT
C15A-O3-C18	121.0(3)	-	N2-C10-C11	111.4(2)	113.8879
C15-O3-C18	118.8(3)	118.4111	O2-C11-N3	124.4(3)	126.1346
C7-N1-C6	119.1(2)	119.5800	O2-C11-C10	121.6(2)	120.7388
C8-N2-C1	122.2(2)	121.6898	N3-C11-C10	114.1(2)	113.1246
C8-N2-C10	117.3(2)	116.8685	C13-C12-C17	120	118.9478
C1-N2-C10	120.5(3)	121.4350	C13-C12-N3	117.0(2)	117.2142
C11-N3-C12A	125.6(3)	-	C17-C12-N3	123.0(2)	123.8379
C11-N3-C12	125.7(3)	128.7956	C14-C13-C12	120	120.8525
C2-C1-N2	123.2(3)	122.8133	C13-C14-C15	120	120.2259
C2-C1-C6	119.7(3)	119.8050	O3-C15-C14	117.9(2)	115.8975
N2-C1-C6	117.1(3)	117.3783	O3-C15-C16	121.7(2)	124.9005
C3-C2-C1	120.1(3)	119.5210	C14-C15-C16	120	119.2019
C2-C3-C4	120.8(3)	121.1098	C17-C16-C15	120	120.6064
C5-C4-C3	120.0(3)	119.5696	C16-C17-C12	120	120.1655
C4-C5-C6	119.8(3)	120.6480	C13A-C12A-C17A	120	-
N1-C6-C5	118.1(3)	118.5774	C13A-C12A-N3	120.9(2)	-
N1-C6-C1	122.3(3)	122.1052	C17A-C12A-N3	119.1(2)	-
C5-C6-C1	119.5(3)	119.3157	C12A-C13A-C14A	120	-
N1-C7-C8	123.3(3)	122.9406	C15A-C14A-C13A	120	-
N1-C7-C9	119.8(3)	120.4617	O3-C15A-C14A	118.4(2)	-
C8-C7-C9	116.8(3)	116.5976	O3-C15A-C16A	121.5(2)	-
O1-C8-N2	122.1(3)	121.3366	C14A-C15A-C16A	120	-
O1-C8-C7	122.1(3)	122.8382	C17A-C16A-C15A	120	-
N2-C8-C7	115.8(2)	115.8170	C16A-C17A-C12A	120	-

Table 5
The contributions of short contacts to Hirshfeld Surface of the molecule (%).

H···H	C···H	O···H	N···H	C···N	N···N	C···C	N···O	C···O
52.6	20.1	19.3	3.6	2.1	0.8	0.9	0.2	0.2

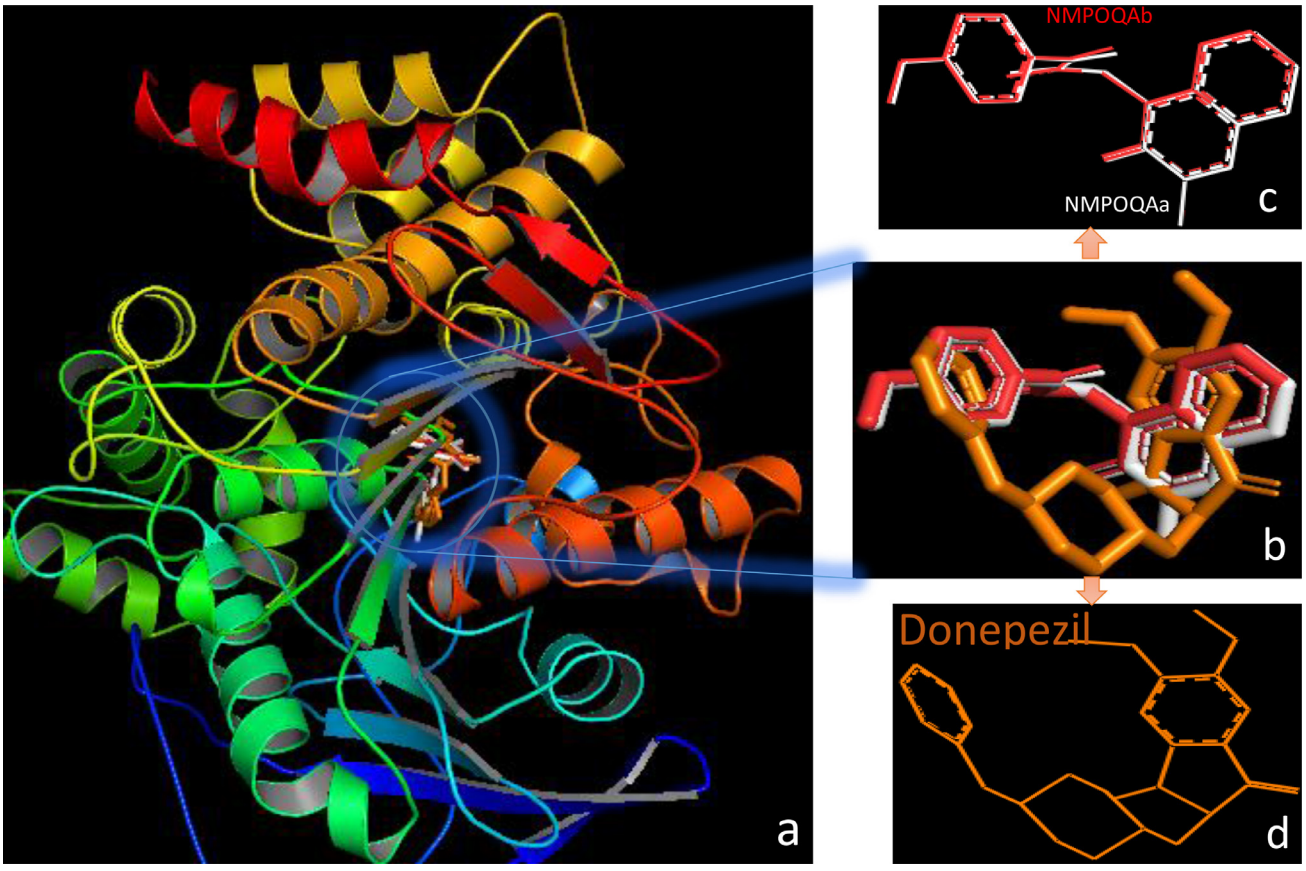

Fig. 7. (a) The superposition of the title ligand (NMPOQAa and NMPOQAb components) (N-(4-methoxyphenyl)-2-(3-methyl-2-oxo-3,4-dihydroquinoxalin-1(2H)-yl)acetamide) and donepezil drug-orange sticks [63] docked under identical conditions against 1EVE protease and represented by PyMOL [7]; (b) The superposition of donepezil and the title ligand (NMPOQAa and NMPOQAb component) without the protease,1EVE, for simplicity and easy comparison; (c) The displays of the NMPOQAa in the active sites of the AChE; (d) The display of the Donepezil drug without 1EVE.

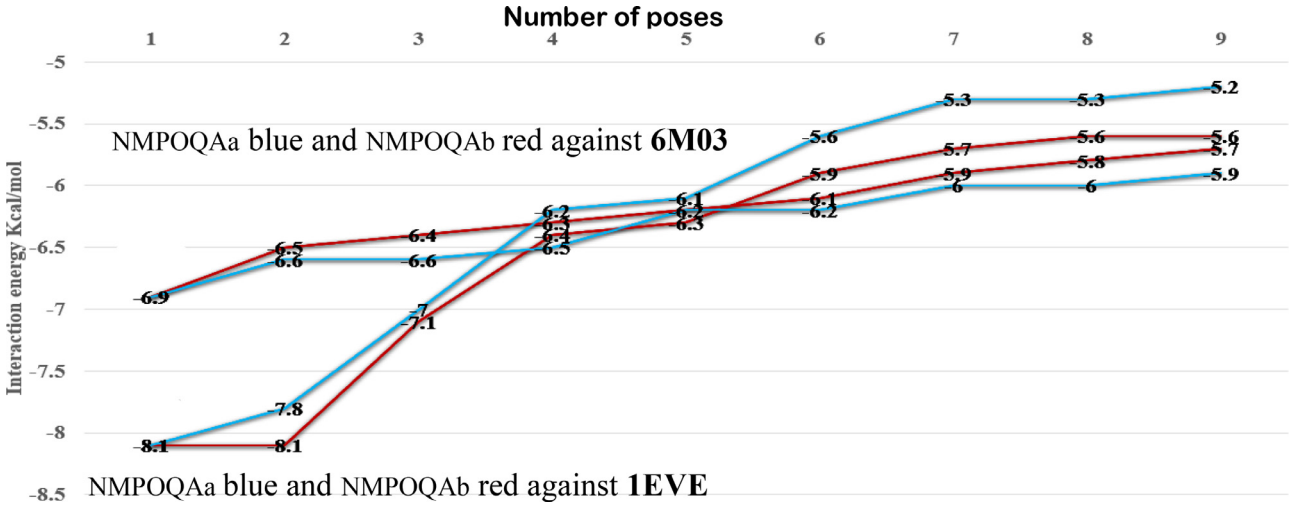

Fig. 8. Analysis docking results of 6M03 and 1EVE against the NMPOQAa and NMPOQAb showing 9 poses each for comparative study.

19, (M^{Pro}, PDB 6M03). Worth mentioning here that different previous docking studies have used 6LQY and 7BQY with various **resolutions** [64,65]. The docked molecule, fitted to interact with the active site of protease 6M03, is shown in Fig. 10(a). Guessing conformational modifications of both the ligand and the 6M03 is a challenge as both show variable degrees of alteration upon binding due to reasons such as hydrophobic interactions, H-bonding, solvation, and more [66]. The conformational changes that are occurred in the protein can be calculated by measuring the torsion angle of the ligand before and after docking using PyMOL [65,56]. The amino acid residue Gln110 shows a H-bond (2.86 Å) with NMPOQAa, Fig. 9(b) whereas amino acid residues Gln110, Asp295 and ser158 show H-bonds with Remdesivir drug, 3.15, 2.922 and 2.85 Å respectively. The NMPOQAa and Remdesivir drug reacted with 6M03 also through many hydrophobic interactions. The common amino acid residues of the active site of the protease 6M03 form hydrophobic interactions include: Phe8, Gln100, Arg105, Asp150 and Asp295. The cut-off for

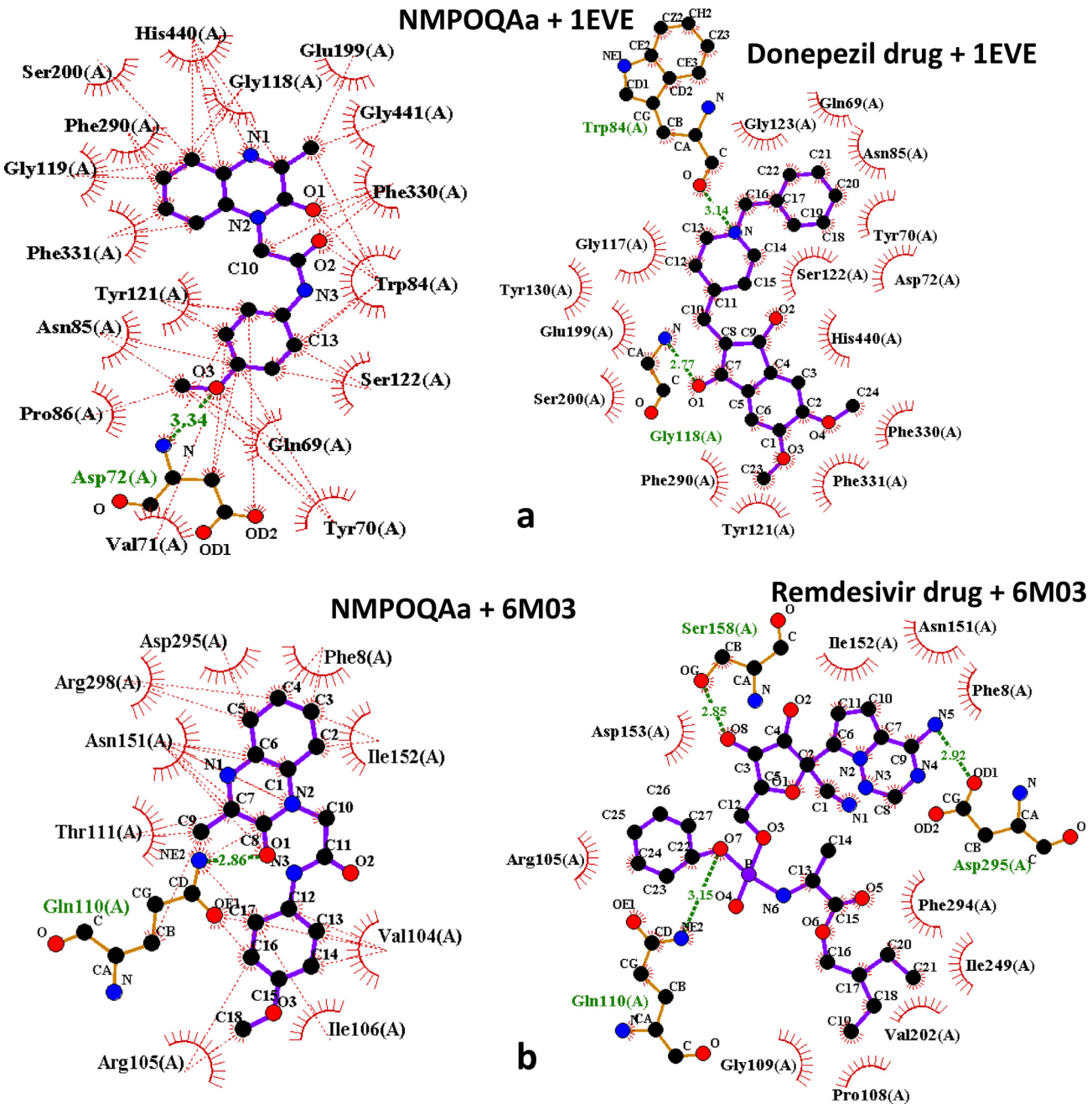

Fig. 9. (a) A schematic 2D LIGPLOT representation of the main protease (M^{pro}; PDB code 1EVE) complex with *N-(4-methoxyphenyl)-2-(3-methyl-2-oxo-3,4-dihydroquinoxalin-1(2H)-yl)acetamide* NMPOQAa*)*. The purple–blue stick, at the centre, represents NMPOQAa and Donepezil drug; (b) The same as for (a) but against the main protease (M^{pro}; PDB code 6M03) complex. The brown solid lines is an active site (residue Asp72) involved in creating a H-bond with the title ligand, NMPOQAa and Remdesivi. The green dashed line represents the hydrogen bonds and the thin red dashed lines represent the hydrophobic residue bonds with the ligand.

the non-bonded interactions, for the LIGPLOTs reported here, is 3.9 Å [55], Fig. 9.

In this study, more light has been shed on the behavior of the two independent molecules (NMPOQAa and NMPOQAb). Binding affinity is an important key to appreciate the strength of the binding interaction between the ligand or Remdesivir drug (the inhibitor) and the 6M03 protease. The binding affinity obtained for our acetamide-base ligand with 6M03 is -6.9 kcal/mol for both molecules NMPOQAa and NMPOQAb in the first pose, however, the remaining poses behaved differently indicating that both the molecules did not behave identically against the protease, Fig. 8. Remdesivir was docked under the same conditions in this study as fr both the independent molecules, Fig. 10. It is possible to see the different displays of NMPOQAa and NMPOQAb, Fig. 9(c) against 6M03.

In general, the molecular docking results of NMPOQA (acetamide-based ligand) compared to the Remdesivir drug, show good matching effective interactions of the proteins with the molecules involving N and O atoms and this could be attributed to the presence of lone pair electrons on these atoms. Also, $\pi\cdots\pi$ stacking is a major contributor in hydrophobic interactions. Furthermore, a close low binding affinity of the NMPOQA (−6.9 kcal/mol. compared to the Remdesivir drug (−7.1 kcal/mol) makes our NMPOQA a good candidate against COVID-19.

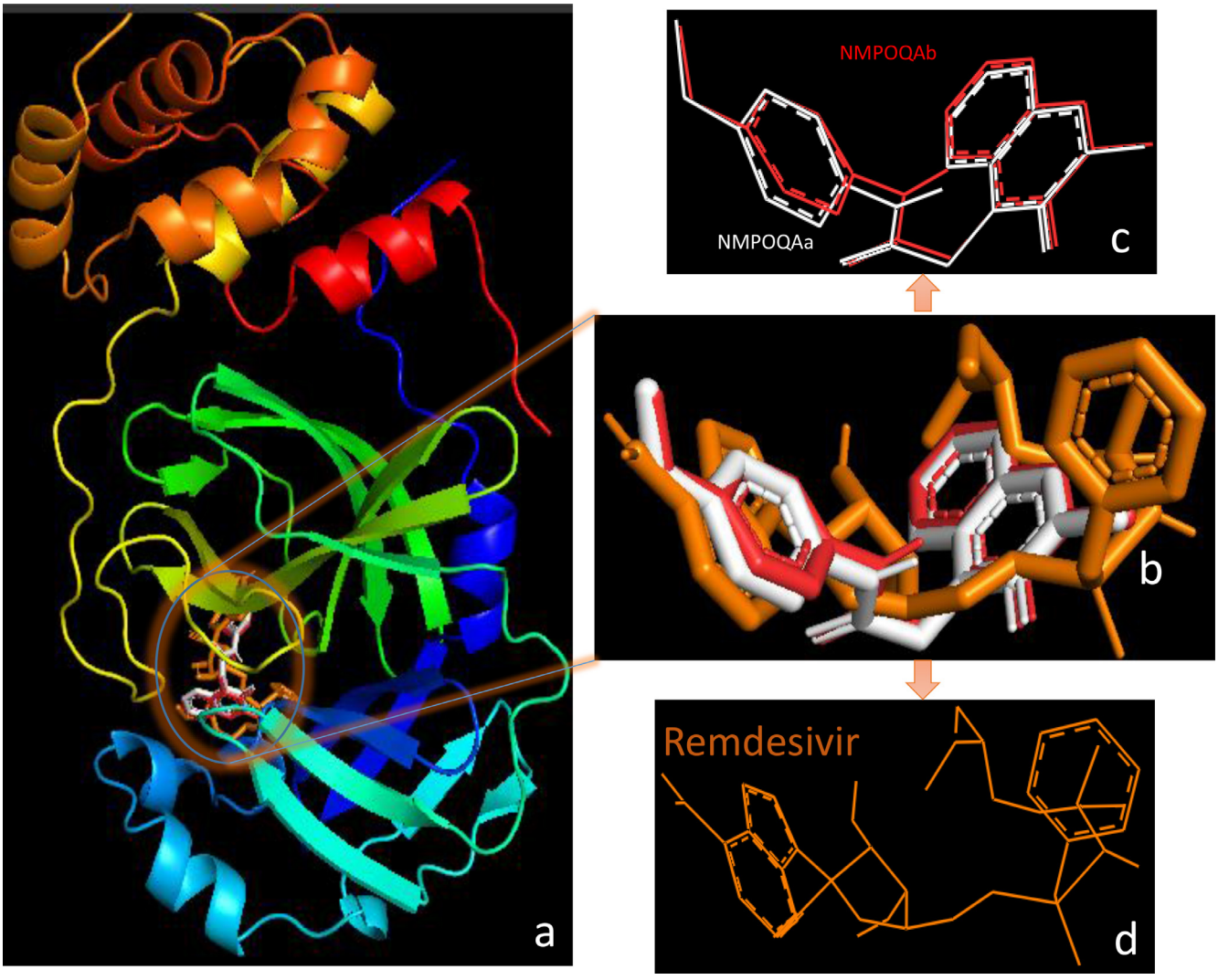

Fig. 10. (a) The superposition of the title ligand (N-(4-methoxyphenyl)-2-(3-methyl-2-oxo-3,4-dihydroquinoxalin-1(2H)-yl)acetamide) and remdesivir drug-orange sticks docked under same conditions against the 6M03 protease and represented by PyMOL [55]; (b) The superposition of remdesivir drug and the title ligand (NMPOQAa and NMPOQAb components) without the protease (6M03) for simplicity and easy comparison; (c) The displays of the NMPOQA in the active sites of the protease; (d) The display of the Remdesivir drug.

4. Conclusion

NMPOQA has been synthesized and characterised via IR, NMR and LC-MS mass spectra. A single crystal was obtained and its structure was investigated by using X-ray diffraction method. This compound crystallizes in the triclinic crystal system with P -1 space group. NMPOQA molecule has disorder at benzene group. Theoretical parameters of the title compound were calculated using DFT method with 6-311++G(d,p) basis set. Although the theoretical parameters close to the experimental parameters, the theoretical geometry doesn't overlap with the experimental geometry because of the difference in torsion angle. MEP and Hirshfeld surface analysis reveals that the molecule has active regions in the environment of oxygen atoms for intermolecular interactions. Furthermore, HOMO-LUMO gap energy was obtained as 3.4841 eV. Molecular docking of NMPOQA and Remdesivir drug with 6M03 was performed showing similar behavior towards COVID-19. A similar study was calculated for NMPOQA with 1EVE producing reasons that suggest our ligand may perhaps merit further study in the context of possible Alzheimer's disease (AD) treatment.

Declaration of Competing Interest

The authors of this manuscript have no conflict of interest to declare.

CRediT authorship contribution statement

Mohcine Missioui: Investigation. **Musa A. Said:** Investigation, Software, Writing – original draft. **Güneş Demirtaş:** Investigation, Software, Writing – original draft. **Joel T. Mague:** Data curation, Formal analysis. **Youssef Ramli:** Conceptualization, Project administration, Methodology, Supervision, Writing – review & editing.

Acknowledgment

Authors are grateful to Mohammed V University and to Ondokuz Mayıs University Research Fund for financial support for this study. The support of NSF-MRI Grant #1228232 for the purchase of the diffractometer and Tulane University for support of the Tulane Crystallography Laboratory are gratefully acknowledged.

Supplementary materials

Supplementary material associated with this article can be found, in the online version, at doi:10.1016/j.molstruc.2021.131420.

References

[1] S.O. Alomari, Z. Abou-Mrad, A. Bydon, COVID-19 and the central nervous system, Clin. Neurol. Neurosurg. 198 (2020) 106116, doi:10.1016/j.clineuro.2020.106116.

[2] H. Wang, R. Qin, J. Zhang, Y. Chen, Possible immunity, inflammation, and oxidative stress mechanisms of Alzheimer's disease in COVID-19 patients, Clin. Neurol. Neurosurg. 201 (2021) 106414, doi:10.1016/j.clineuro.2020.106414.

[3] R. Lu, W. Wang, X. Li, Combined with western medicine conventional therapy in the treatment of 63 suspected cases of Coronavirus Disease 2019, J. Tradit. Chin. Med. 61 (2020) 655–659.

[4] L. Runfeng, H. Yunlong, H. Jicheng, P. Weiqi, M. Qinhai, S. Yongxia, L. Chufang, Z. Jin, J. Zhenhua, J. Haiming, Z. Kui, H. Shuxiang, D. Jun, L. Xiaobo, H. Xiaotao, W. Lin, Z. Nanshan, Y. Zifeng, Lianhuaqingwen exerts anti-viral and anti-inflammatory activity against novel coronavirus (SARS-CoV-2), Pharmacol. Res. 156 (2020) 104761, doi:10.1016/j.phrs.2020.104761.

[5] Y.W. David Lee, Y. Qing Li, J. Liu, T. Efferth, Traditional Chinese herbal medicine at the forefront battle against COVID-19: clinical experience and scientific basis, Phytomedicine 80 (2021) 153337, doi:10.1016/j.phymed.2020.153337.

[6] Y. Xiong, M. Gao, B. Duijn, H. Choi, F. Horssen, M. Wang, International policies and challenges on the legalization of traditional medicine/herbal medicines in the fight against COVID-19, Pharmacol. Res., doi:10.1016/j.phrs.2021.105472.

[7] B. Cao, Y. Wang, D. Wen, W. Liu, J. Wang, G. Fan, et al., A trial of lopinavir–ritonavir in adults hospitalized with severe COVID-19, N. Engl. J. Med. 382 (2020) 1787–1799, doi:10.1056/NEJMoa2001282.

[8] O. Sogut, M.M. Can, R. Guven, O. Kaplan, H. Ergenc, T.B. Umit, O. Demir, M. Kaya, T. Akdemir, S. Cakmak, Safety and efficacy of hydroxychloroquine in 152 outpatients with confirmed COVID-19: a pilot observational study, Am. J. Emerg. Med. 40 (2021) 41–46, doi:10.1016/j.ajem.2020.12.014.

[9] F. Cantini, L. Niccoli, D. Matarrese, E. Nicastri, P. Stobbione, D. Goletti, Baricitinib therapy in COVID-19: a pilot study on safety and clinical impact, J. Infect. 81 (2020) 318–356, doi:10.1016/j.jinf.2020.04.017.

[10] C.D. Russell, J.E. Millar, J.K. Baillie, Clinical evidence does not support corticosteroid treatment for 2019-nCoV lung injury, Lancet 395 (2020) 473–475, doi:10.1016/S0140-6736(20)30317-2.

[11] L. Pasin, G. Cavalli, P. Navalesi, N. Sella, G. Landoni, G. Yavorovskiy, V. Valery, A Zangrillo, L. Dagna, G. Monti, Anakinra for patients with COVID-19: a meta-analysis of non-randomized cohort studies, Eur. J. Internal Med. 86 (2021) 34–40, doi:10.1016/j.ejim.2021.01.016.

[12] G. Cavalli, G. De Luca, C. Campochiaro, E. Della Torre, M. Roipa, D. Canetti, et al., Interleukin-1 blockade with high-dose anakinra in patients with COVID-19, acute respiratory distress syndrome, and hyperinflammation: a retrospective cohort stud, Lancet Rheumatol. 2 (2020) 325–331, doi:10.1016/S2665-9913(20)30127-2.

[13] J.M. Sanders, M.L. Monogue, T.Z. Jodlowski, et al., JAMA 323 (2020) 1824–1836, doi:10.1001/jama.2020.6019.

[14] P. Luo, Y. Liu, L. Qiu, X. Liu, D. Liu, J. Li, Tocilizumab treatment in COVID-19: a single center experience, J. Med. Virol. 92 (2020) 814–818, doi:10.1002/jmv.25801.

[15] M. Colaneri, L. Bogliolo, P. Valsecchi, P. Sacchi, V. Zuccaro, F. Brandolino, et al., Tocilizumab for Treatment of Severe COVID-19 Patients: Preliminary Results from SMAtteo COvid19 REgistry (SMACORE), Microorganisms 8 (2020) 695, doi:10.3390/microorganisms8050695.

[16] L. Quartuccio, A. Sonaglia, D. McGonagle, M. Fabris, M. Peghin, D. Pecori, et al., Profiling COVID-19 pneumonia progressing into the cytokine storm syndrome: results from a single Italian Centre study on tocilizumab versus standard of care, J. Clin. Virol. 129 (2020) 104444, doi:10.1016/j.jcv.2020.104444.

[17] C. Campochiaro, E. Della-Torre, G. Cavalli, G. De Luca, M. Ripa, N. Boffini, et al., Efficacy and safety of tocilizumab in severe COVID-19 patients: a single-centre retrospective cohort study, Eur. J. Intern. Med. 76 (2020) 43–49, doi:10.1016/j.ejim.2020.05.021.

[18] W. Zhang, Y. Zhao, F. Zhang, Q. Wang, T. Li, Z. Liu, et al., The use of antiinflammatory drugs in the treatment of people with severe coronavirus disease 2019 (COVID-19): the perspectives of clinical immunologist from China, Clin. Immunol. 214 (2020), doi:10.1016/j.clim.2020.108393.

[19] C. Zhang, S. Huang, F. Zheng, Y. Dai, Controversial treatments: an updated understanding of the coronavirus disease 2019, J. Med. Virol. (2020), doi:10.1002/jmv.25788.

[20] Z. Yang, J. Liu, Y. Zhou, X. Zhao, Q. Zhao, J. Liu, The effect of corticosteroid treatment on patients with coronavirus infection: a systematic review and metaanalysis, J. Infect. 81 (2020) e13–e20, doi:10.1016/j.jinf.2020.03.062.

[21] N. Veronese, J. Demurtas, L. Yang, et al., Use of corticosteroids in coronavirus disease 2019 pneumonia: a systematic review of the literature, Front. Med. 7 (2020) 170, doi:10.3389/fmed.2020.00170.

[22] Z. Ye, Y. Wang, L.E. Colunga-Lozano, et al., Efficacy and safety of corticosteroids in COVID-19 based on evidence for COVID-19, other coronavirus infections, influenza, community-acquired pneumonia and acute respiratory distress syndrome: a systematic review and meta-analysis, CMAJ 192 (2020) E756–E767, doi:10.1503/cmaj.200645.

[23] M. Parsey, An open letter from Merdad Parsey, Chief Medical Officer, Gilead Sciences, 2020. https://stories.gilead.com/articles/open-letter-from-merdad-par sey, (Accessed 22 October 2020).

[24] and Y. Ramli, E. M. Essassi, advances in synthetic approaches, functionalization and biological properties of quinoxaline derivatives, in: J.C. Taylor (Ed.), Advances in Chemistry Research, 27, Nova Science Publishers, New York, 2015, pp. 109–160.

[25] Y. Ramli, A. Moussaif, K. Karrouchi, E.M. Essassi, Pharmacological profile of quinoxalinone, J. Chem. (2014) 2014 Article 563406; https://doi.org/10.1155/2014/563406. 8.

[26] A. Zarrouk, H. Zarrok, Y. Ramli, M. Bouachrine, B. Hammouti, A. Sahibeddinee, F. Bentisse, Inhibitive properties, adsorption and theoretical study of 3,7-dimethyl-1-(prop-2-yn-1-yl)quinoxalin2(1H)-one as efficient corrosion inhibitor for carbon steel in hydrochloric acid solution, J. Mol. Liq. 222 (2016) 239–252, doi:10.1016/j.molliq.2016.07.046.

[27] S. Srinivasarao, A. Nandikolla, A. Kopec Ewa, A. Suresh, A. Głogowska, B. Ghosh, B. Karan Kumar et, Discovery of 1, 2, 3-triazole based quinoxaline-1, 4-di-N-oxide derivatives as potential anti-tubercular agents, Bioorg. Chem. 100 (2020) 103955, doi:10.1016/j.bioorg.2020.103955.

[28] H.M. Patel, V. Bhardwaj, P. Sharma, M.N. Noolvi, S. Lohan, S. Bansal, A. Sharma, Quinoxaline-PABA bipartite hybrid derivatization approach: design and search for antimicrobial agents, J. Mol. Struct. 1184 (2019) 562–568, doi:10.1016/j.molstruc.2019.02.074.

[29] C.-B. Zheng, W.-C. Gao, P.-P. Pang, X. Ma, L.-C. Peng, L. Yang, X. Li, Synthesis and vasorelaxant evaluation of novel 7-methoxyl-2,3-disubstituted-quinoxaline derivatives, Bioorg. Med. Chem. Lett. 36 (2021) 127785, doi:10.1016/j.bmcl.2021.127785.

[31] D. Dewangan, K.T. Nakhate, V.S. Verma, K. Nagori, H. Badwaik, N. Nair, D. Krishna Tripathi, A. Mishra, Synthesis and molecular docking study of novel hybrids of 1, 3, 4-oxadiazoles and quinoxaline as a potential analgesic and anti-inflammatory agents, J. Heterocycl. Chem. 55 (2018) 2901–2910, doi:10.1002/jhet.3363.

[32] Q.K. Shen, G.H. Gong, G. Li, M. Jin, L.H. Cao, Z.S. Quan, Discovery and evaluation of novel synthetic 5-alkyl-4-oxo-4, 5-dihydro-[1, 2, 4] triazolo [4, 3-a] quinoxaline-1-carbox-amide derivatives as anti-inflammatory agents., J. Enzyme Inhib. Med. 35 (2020) 85–95, doi:10.1080/14756366.2019.1680658.

[30] D.D. Guerreiro, L. Ferreira de Lima, N. Arcângela Ribeiro de Sá, G. Tetaping Mbemya, A. Clara Accioly Ferreira, B. Geraldo Alves, S. Sant'anna Maranhão et, Response of preantral follicles exposed to quinoxaline: a new compound with anticancer potential, Res. Vet. Sci. 128 (2020) 261–268, doi:10.1016/j.rvsc.2019.12.010.

[33] H. Zhang, J. Zhang, W. Qu, S. Xie, L. Huang, D. Chen, Y. Tao, Z. Liu, Y. Pan, Z. Yuan, Design, synthesis, and biological evaluation of novel thiazolidinone–containing quinoxaline-1,4-di-N-oxides as antimycobacterial and antifungal agents, Front. Chem. 8 (2020) 598, doi:10.3389/fchem.2020.00598.

[34] S.B. Patel, B.D. Patel, C. Pannecouque, H.G. Bhatt, Design, synthesis and anti-HIV activity of novel quinoxaline derivatives, Eur. J. Med. Chem. 117 (2016) 230–240, doi:10.1016/j.ejmech.2016.04.019.

[35] N. Husna Ibrahim, M.F. Yahaya, W. Mohamed, S.L. Teoh, C.K. Hui, J. Kumar, Pharmacotherapy of Alzheimer's disease: seeking clarity in a time of uncertainty, Front. Pharmacol. 11 (2020) 261, doi:10.3389/fphar.2020.00261.

[36] Y. Zaoui, Y. Ramli, S.L. Tan, E.R.T. Tiekink, L. Chemlal, J.T. Mague, J. Taoufik, M.E.A. Faouzi, M.H. Ansar, Synthesis, structural characterisation and theoretical studies of a novel pyridazine derivative: investigations of anti-inflammatory activity and inhibition of α-glucosidase, J. Mol. Struct. 1234 (2021) 130177, doi:10.1016/j.molstruc.2021.130177.

[37] N. Abad, H.H. Sallam, F.H. Al-Ostoot, H.A. Khamees, S.A. Al-horaibi, S. A.Khanum, M. Madegowda, M. El Hafi, J.T. Mague, E. M.Essassi, Y. Ramli, Synthesis, crystal structure, DFT calculations, Hirshfeld surface analysis, energy frameworks, molecular dynamics and docking studies of novel isoxazole-quinoxaline derivative (IZQ) as anti-cancer drug, J. Mol. Struct. 1232 (2021) 130004, doi:10.1016/j.molstruc.2021.130004.

[38] N. Abad, S. Ferfra, E.M. Essassi, J.T. Mague, Y. Ramli, Synthesis and crystal structure of 1-octyl-3-phenylquinoxalin-2 (1H)-one, C22H26N2O, Z. Kristallogr. NCS 236 (2021) 173–175, doi:10.1515/ncrs-2020-0404.

[39] W. Guerrab, M. Missioui, Y. Zaoui, J.T. Mague, Y. Ramli, Synthesis and crystal structure of 2-azido-N-phenylacetamide, $C_8H_8N_4O$, Z. Kristallogr. NCS 236 (2021) 133–134, doi:10.1515/ncrs-2020-0409.

[40] W. Guerrab, H. Lgaz, S. Kansiz, J.T. Mague, N. Dege, M. Ansar, R. Marzouki, J. Taoufik, I.H. Ali, I.M. Chung, Y. Ramli, Synthesis of a novel phenytoin derivative: crystal structure, Hirshfeld surface analysis and DFT calculations, J. Mol. Struct. 1205 (2019) 127630, doi:10.1016/j.molstruc.2019.127630.

[41] M. Missioui, S. Mortada, W. Guerrab, G. Serdaroglu, S. Kaya, J.T. Mague, E.M. Essassi, M.E.A. Faouzi, Y. Ramli, Novel antioxidant quinoxaline derivative: Synthesis, crystal structure, theoretical studies, antidiabetic activity and molecular docking study, J. Mol. Struct. 1239 (2021) 130484, doi:10.1016/j.molstruc.2021.1304840.

[42] O. Hinsberg, Liebigs Ann. Chem. 237 (1887) 1228.

[43] Bruker*APEX3, SAINT, SADABS* & *SHELXTL*, Bruker AXS, Inc., Madison, WI, 2016.

[44] G.M. Sheldrick, Integrated space-group and crystal-structure determination, Acta Cryst. A71 (2015) 3–8.

[45] G.M. Sheldrick, Crystal structure refinement with *SHELXL*, Acta Cryst. C71 (2015) 3–8.

[46] K. Brandenburg, H. Putz, DIAMOND, Crystal Impact GbR, Bonn, Germany, 2012.

[47] G.M. Sheldrick, TWINABS, University of Göttingen, Göttingen, Germany, 2009.

[48] J.R.C.M.J. Frisch, G.W. Trucks, H.B. Schlegel, G.E. Scuseria, M.A. Robb, S.S.I.J.A. Montgomery Jr., T. Vreven, K.N. Kudin, J.C. Burant, J.M. Millam, G.A.P.J. Tomasi, V. Barone, B. Mennucci, M. Cossi, G. Scalmani, N. Rega, T.H. Nakatsuji, M. Hada, M. Ehara, K. Toyota, R. Fukuda, J. Hasegawa, M. Ishida, H.P.H. Nakajima, Y. Honda, O. Kitao, H. Nakai, M. Klene, X. Li, J.E. Knox, A.J.J.B. Cross, C. Adamo, J. Jaramillo, R. Gomperts, R.E. Stratmann, O. Yazyev, G.A. Austin, R. Cammi, C. Pomelli, J.W. Ochterski, P.Y. Ayala, K. Morokuma, A.D.D. Voth, P. Salvador, J.J. Dannenberg, V.G. Zakrzewski, S. Dapprich, J.B.F.M.C. Strain, O. Farkas, D.K. Malick, A.D. Rabuck, K. Raghavachari, A.J.V. Ortiz, Q. Cui, A.G. Baboul, S. Clifford, J. Cioslowski, B.B. Stefanov, G. Liu, M.A.A.-L. Liashenko, P. Piskorz, I. Komaromi, R.L. Martin, D.J. Fox, T. Keith, W.C.C.Y. Peng, A. Nanayakkara, M. Challacombe, P.M.W. Gill, B. Johnson, J.A.P.M.W. Wong, C. Gonzalez, Gaussian 03, Revision C.02, Gaussian, Inc., Wallingford CT, 2004.

[49] Æ. Frisch, R.D. Dennington II, T.A. Keith, J. Millam, A.B. Nielsen, A.J. Holder, J. Hiscocks, GaussView 4 (2007) www.gaussian.com.

[50] M.A. Turner, M.J. Mckinnon, J.J. Wolff, S.K. Grimwood, D.J. Grimwood, D.J. Spackman, P.R. Jayatilaka, D. Spackman, CrystalExplorer. Version 17. The University of Western Australia, CrystalExplorer. Version 17, Univ. West. Aust. 2017 (2017).

[51] S.T. Tanoli, M. Ramzan, A. Hassan, A. Sadiq, M.S. Jan, F.A. Khan, F. Ullah, H. Ahmad, M. Bibi, T. Mahmood, U. Rashid, Y.A. Rodríguez Núñez, M. Gutíerrez, J. Alzate-Morales, F. Adasme-Carreño, F.M. Güiza, C.C. Bernal, A.R. Romero Bohórquez, P. Synthesis, M. Docking, D.F.T. Studies, A. Rivera, Design, synthesis and bioevaluation of tricyclic fused ring system as dual binding site acetylcholinesterase inhibitors, Int. J. Mol. Sci. 83 (2020) 1–25, doi:10.1016/j.bioorg.2018.10.035.

[52] O. Trott, A.J. Olson, AutoDock Vina: improving the speed and accuracy of docking with a new scoring function, efficient optimization, and multithreading, J. Comput. Chem. 31 (2009) 455–461, doi:10.1002/jcc.21334.

[53] A. Allouche, Software news and updates gabedit — a graphical user interface for computational chemistry softwares, J. Comput. Chem. 32 (2012) 174–182, doi:10.1002/jcc.

[54] B.G. Samy, L. Xavier, Molecular docking studies on antiviral drugs for SARS, Int. J. Adv. Res. Comput. Sci. Softw. Eng. 5 (2015) 75–79.

[55] A.C. Wallace, R.A. Laskowski, J.M. Thornton, Ligplot: A program to generate schematic diagrams of protein-ligand interactions, Protein Eng. Des. Sel. 8 (1995) 127–134, doi:10.1093/protein/8.2.127.

[56] W.L. DeLano, PyMOL Reference Guide, Delano Sci, San Carlos, CA, US, 2004.

[57] I. Fleming, J. Wiley, Frontier orbitals and organic chemical reactions, J. Mol. Struct. 56 (1979) 306, doi:10.1016/0022-2860(79)80172-6.

[58] S. Prasad, D.P. Ojha, Vibrational spectra, electronic properties and effect of alkyl chain length on chemical stability of nematogens – a comparision using DFT and HF methods, Mol. Cryst. Liq. Cryst. 658 (2017) 69–80, doi:10.1080/15421406.2017.1415656.

[59] D.F.V. Lewis, C. Ioannides, D.V. Parke, Interaction of a series of nitriles with the alcohol-inducible isoform of P450: computer analysis of structure—activity relationships, Xenobiotica 24 (1994) 401–408, doi:10.3109/00498259409043243.

[60] S. Murugavel, V. Vetri Velan, D. Kannan, M. Bakthadoss, Synthesis, crystal structure analysis, spectral investigations, DFT computations, biological activities and molecular docking of methyl(2E)-2-{[N-(2-formylphenyl)(4-methylbenzene) sulfonamido]methyl}-3-(4-fluorophenyl)prop-2-enoate, a potential bioactive, J. Mol. Struct. 1108 (2016) 150–167, doi:10.1016/j.molstruc.2015.11.047.

[61] K.P. Kepp, Bioinorganic chemistry of Alzheimer's disease, Chem. Rev. 112 (2012) 5193–5239, doi:10.1021/cr300009x.

[62] G. Aljohani, A.A.S. Ali, M.A. Said, D.L. Hughes, S.Y. Alraqa, S. Amran, F. Ahmad, N. Basar, 2-Benzyloxynaphthalene aminoalkylated chalcone designed as acetylcholinesterase inhibitor: structural characterisation, in vitro biological activity and molecular docking studies, J. Mol. Struct. 1222 (2020) 128898, doi:10.1016/j.molstruc.2020.128898.

[63] A. Shamsi, M. Al Shahwan, S. Ahamad, M.I. Hassan, F. Ahmad, A. Islam, Spectroscopic, calorimetric and molecular docking insight into the interaction of Alzheimer's drug donepezil with human transferrin: implications of Alzheimer's drug, J. Biomol. Struct. Dyn. 38 (2020) 1094–1102, doi:10.1080/07391102.2019.1595728.

[64] Z. Jin, X. Du, Y. Xu, Y. Deng, M. Liu, Y. Zhao, B. Zhang, X. Li, L. Zhang, C. Peng, Y. Duan, J. Yu, L. Wang, K. Yang, F. Liu, R. Jiang, X. Yang, T. You, X. Liu, X. Yang, F. Bai, H. Liu, X. Liu, L.W. Guddat, W. Xu, G. Xiao, C. Qin, Z. Shi, H. Jiang, Z. Rao, H. Yang, Structure of Mpro from SARS-CoV-2 and discovery of its inhibitors, Nature 582 (2020) 289–293, doi:10.1038/s41586-020-2223-y.

[65] M.A. Alsafi, D.L. Hughes, M.A. Said, First COVID-19 molecular docking with a chalcone-based compound: synthesis, single-crystal structure and Hirshfeld surface analysis study, Acta Crystallogr. Sect. C Struct. Chem. 76 (2020) 1043–1050, doi:10.1107/s2053229620014217.

[66] F. Stephanie, A.H. Alkaff, U.S.F. Tambunan, Flexible molecular docking simulation of peptide compounds as inhibitor of GluI host protein for dengue fever therapy, AIP Conf. Proc. 2237 (2020), doi:10.1063/5.0005237.